Numerical simulation of time delay interferometry for TAIJI and new LISA

RAA 2019 Vol. **19** No. **4**, 58(14pp) doi: 10.1088/1674–4527/19/4/58

http://www.raa-journal.org *http://iopscience.iop.org/raa*

***R**esearch in*
***A**stronomy and*
***A**strophysics*

Numerical simulation of time delay interferometry for TAIJI and new LISA

Gang Wang[1,2] and Wei-Tou Ni[3,4]

[1] INFN, Gran Sasso Science Institute, I-67100 L'Aquila, Italy; *gwanggw@gmail.com*
[2] INFN, Sezione di Pisa, Edificio C, Largo Bruno Pontecorvo, 3, I-56127, Pisa, Italy
[3] National Astronomical Observatories, Chinese Academy of Sciences, Beijing 100101, China; *weitou@gmail.com*
[4] State Key Laboratory of Magnetic Resonance and Atomic and Molecular Physics, Wuhan Institute of Physics and Mathematics, Chinese Academy of Sciences, Wuhan 430071, China

Received 2018 September 4; accepted 2018 October 31

Abstract The success of LISA Pathfinder in demonstrating the LISA drag-free requirement paved the way for using space interferometers to detect low-frequency and middle-frequency gravitational waves (GWs). The TAIJI GW mission and the new LISA GW mission propose using an arm length of 3 Gm ($1\,\mathrm{Gm} = 10^6\,\mathrm{km}$) and an arm length of 2.5 Gm respectively. For a space laser-interferometric GW antenna, due to astrodynamical orbit variation, time delay interferometry (TDI) is needed to achieve nearly equivalent equal-arms for suppressing the laser frequency noise below the level of optical path noise, acceleration noise, etc in order to attain the requisite sensitivity. In this paper, we simulate TDI numerically for the TAIJI mission and the new LISA mission. To do this, we work out a set of 2200-day (6-year) optimized science orbits for each mission starting on 2028 March 22 using the CGC 2.7.1 ephemeris framework. Then we use the numerical method to calculate the residual optical path differences of the first-generation TDI configurations and the selected second-generation TDI configurations. The resulting optical path differences of the second-generation TDI configurations calculated for TAIJI, new LISA and eLISA are well below their respective requirements for laser frequency noise cancelation. However, for the first-generation TDI configurations, the original requirements need to be relaxed by 3 to 30 fold to be satisfied. For TAIJI and the new LISA, about one order of magnitude relaxation would be good and recommended; this could be borne on the laser stability requirement in view of recent progress in laser stability, or the GW detection sensitivities of the second-generation TDIs have to be used in the diagnosis of the observed data instead of the commonly used X, Y and Z TDIs.

Key words: gravitational waves — methods: numerical — techniques: interferometric

1 INTRODUCTION AND SUMMARY

Gravitational wave (GW) detection has been a focus of research for several decades. In all GW frequency bands, detection efforts are pursued vigorously (see, e.g. Kuroda et al. 2015). With the announcement of advanced LIGO and Virgo direct GW detection (Abbott et al. 2016b,a, 2017a,c,d,b), we are in the age of GW astronomy.

1.1 Space Laser-interferometric GW Detectors

Space laser-interferometric GW detectors operate in the low frequency band (100 nHz–0.1 Hz) and the middle frequency band (0.1–10 Hz). The scientific goals are to detect the following GW sources in these bands: (i) Supermassive black holes (BHs); (ii) Extreme mass ratio inspirals; (iii) Intermediate-mass BHs; (iv) Compact binaries; (v) Relic GWs, and to use observation and measurement of these sources to study the co-evolution of supermassive BHs with galaxies to anticipate binary merging GW events in the high frequency band (10 Hz–100 kHz) for Earth-based GW detection, to test relativistic gravity, to determine cosmological parameters and to study the dark energy equation of state. Space-borne GW detectors may provide a much higher signal-to-noise ratio for GW detection than Earth-based detectors.

Interferometric GW detection in space basically measures the difference in the distances traveled through two routes of laser links among spacecraft (S/C) or celestial bodies as GWs pass by. The S/Cs (or celestial bodies) must be in geodesic motion (or such motion can be deduced). The distance measurement must be ultra-sensitive as the GWs are weak. Therefore, drag-free technology to guarantee the geodesic motion and laser stabilization to ensure the required level of measurement are essential to achieve the scientific goals. On the other hand, due to the long distance between S/C in space GW missions, an appropriate amplification method between laser links is also crucial for performing the measurement. This is achieved by either homodyne or heterodyne optical phase locking the local oscillator to the incoming weak light at the received link.

Launched on 2015 December 3, Laser Interferometer Space Antenna (LISA) Pathfinder (Armano et al. 2016) has completely met the stringent LISA drag-free demand (Amaro-Seoane et al. 2017), and has successfully demonstrated the drag-free technology for space detection of GWs.

Liao et al. (2002b,a) and Dick et al. (2008) have demonstrated homodyne phase-locking to 2 pW incoming weak light and offset phase locking to 40 fW incoming laser light respectively. Gerberding et al. (2013) and Francis et al. (2014) have recently phase-locked a 3.5 pW light signal and a 30 fW light signal respectively. LISA requires 85 pW laser light phase locking. Hence, the locking power requirement is demonstrated in laboratories. Frequency-tracking, coding-decoding and modulation-demodulation need to be well-developed in the future to make it a mature technology.

To reach the measurement sensitivity goal for space detection, we need to suppress spurious noise below the target sensitivity level. This requires us to reduce laser noise as much as possible. The drag-free technology has now been demonstrated by LISA Pathfinder. Nevertheless, the best laser stabilization alone is not currently enough to directly reduce the laser noise to the required strain sensitivity of 10^{-21}. To lessen the laser frequency noise requirement, time delay interferometry (TDI) has come to the rescue.

1.2 Time Delay Interferometry

For drag-free S/C, the interferometric arm lengths vary according to astrodynamics. Laser noise must be suppressed below other noises such as the optical path noise, acceleration noise, etc to attain the requisite sensitivity. In order to suppress laser frequency noise, it is necessary to use TDI to match the optical path length in different beam paths closely in the analysis.

Except for DECIGO (Kawamura et al. 2006, 2011) whose arm lengths are controlled, all other space-borne GW interferometers have their arm lengths vary geodetically (in free fall) according to orbital dynamics. The TDI technique uses two different optical paths with sufficiently close optical path lengths and follows them in opposite/different order. This way the laser frequency noise is suppressed when the optical path lengths (time traveled) between the two paths are close enough.

Ni et al. (1997); Ni (1997) first used TDI to study the ASTROD mission concept in the 1990s numerically using Newtonian dynamics. The two TDI configurations are the unequal arm Michelson TDI configuration and the Sagnac TDI configuration for three S/C. The principle is for two split laser beams to go to Paths 1 and 2 and to interfere at the end of their paths. For the unequal arm Michelson TDI configuration, the two paths are

$$\begin{aligned} &\mathrm{Path\ 1: S/C1 \to S/C2 \to S/C1 \to S/C3 \to S/C1},\\ &\mathrm{Path\ 2: S/C1 \to S/C3 \to S/C1 \to S/C2 \to S/C1}. \end{aligned} \tag{1}$$

In the Sagnac TDI configuration, the two paths are

$$\begin{aligned} &\mathrm{Path\ 1: S/C1 \to S/C2 \to S/C3 \to S/C1},\\ &\mathrm{Path\ 2: S/C1 \to S/C3 \to S/C2 \to S/C1}. \end{aligned} \tag{2}$$

After that we performed numerical simulation of the TDI using post-Newtonian ephemeris for ASTROD-GW with no inclination (Wang & Ni 2012, 2013b), LISA (Dhurandhar et al. 2013), eLISA/NGO (Wang & Ni 2013a), LISA-type with 2 Gm arm length (Wang & Ni 2013a) and ASTROD-GW with inclinations (Wang & Ni 2015).

These two configurations are first-generation in the sense of Armstrong et al. (1999) for LISA. For a thorough discussion on the generations and other aspects of TDI, see Tinto & Dhurandhar (2014).

1.2.1 X, Y, Z, X + Y + Z, Sagnac and other first-generation TDIs

The unequal arm Michelson TDI starting from S/C1 is frequently denoted by the symbol X. That starting from S/C2 with $(1, 2, 3)$ permutation in S/C is frequently denoted by the symbol Y, and the one starting from S/C3 by the symbol Z. The Sagnac configuration is frequently denoted by the symbol α, and those with successive permutation(s) by the symbols β and γ. We shall adopt this notation, first used in Armstrong et al. (1999).

Following our previous work (Wang & Ni (2015)) for the numerical evaluation, we take a common receiving time epoch for both beams to calculate the path differences; in this case, the results would be very close to the calculations which we take for the common sending time epoch. This way, we can start from Path 1 and propagate the laser light to the end of Path 1 using the ephemeris framework, and at the end point of Path 1, evolve laser light back in time along the reversed Path 2 to find the difference in the optical path length.

In the TDI, we actually compare the laser signal this way. The results of this calculation for the first-generation TDI for various orbit configurations are shown in Figures 5–8 in Section 3, and their min, max and root mean square (rms) path length differences for a period of 2200 d are compiled in Table 1 of this section; those for the second-generation are shown in Figures 9–12 in Section 4 and the min, max and rms path length differences are compiled in Table 2. To be concise, to denote the second-generation TDIs, the path S/C1 → S/C2 → S/C1 is notated as a and the path S/C1 → S/C3 → S/C1 is notated as b as done in Dhurandhar et al. (2010, 2013) and in Wang & Ni (2013a,b, 2015). Therefore, the difference ΔL between Path 1 and Path 2 for the unequal arm Michelson X could be denoted as $ab - ba \equiv [a, b]$. To extend this notation to the cyclically permuted paths, we refer to
the path S/C2 → S/C3 →S/C2 as c,
the path S/C2 → S/C1 → S/C2 as d,
the path S/C3 → S/C1 → S/C3 as e and
the path S/C3 → S/C2 → S/C3 as f.

Unequal arm Michelson (X, Y, Z), Sagnac (α, β, γ), Relay (U, V, W), Beacon (P, Q, R) and Monitor (E, F, G) configurations are the first-generation TDIs which we calculate numerically in this paper. U, P, and E TDI configurations in geometric representation are given in Vallisneri (2005). They are drawn in Figure 1 with S/C numbers. Two other configurations of each type having different S/C as initial points can be readily figured out by permutation.

1.2.2 Second-generation TDIs

There are many second-generation TDI configurations. In this work, we select $n = 1$ and $n = 2$ configurations which were obtained by Dhurandhar et al. (2010) assuming one detector with two arms for LISA. These configurations for S/C1 as the starting point are listed as follows:

$$\text{(I)} n = 1, [ab, ba] (= abba - baab),$$

$$\text{(II)} n = 2, [a^2b^2, b^2a^2], [abab, baba]; [ab^2a, ba^2b].$$

For S/C2 and S/C3 as the starting points, the TDI configurations are respectively

$$\text{(III)}\ n = 1, [cd, dc],$$

$$\text{(IV)}\ n = 2, [c^2d^2, d^2c^2]; [cdcd, dcdc]; [cd^2c, dc^2d],$$

$$\text{(V)}\ n = 1, [ef, fe],$$

$$\text{(VI)}\ n = 2, [e^2f^2, f^2e^2]; [efef, fefe]; [ef^2e, fe^2f].$$

A second-generation TDI that involves three arms is the following Sagnac-type TDI. From the first-generation Sagnac-α configuration, we add another Sagnac-α in reverse order to get a new interferometry path as follows:

$$\begin{aligned} \text{Path 1} &: \text{S/C1} \to \text{S/C2} \to \text{S/C3} \to \text{S/C1} \\ &\quad \to \text{S/C3} \to \text{S/C2} \to \text{S/C1}, \\ \text{Path 2} &: \text{S/C1} \to \text{S/C3} \to \text{S/C2} \\ &\quad \to \text{S/C1} \to \text{S/C2} \to \text{S/C3} \to \text{S/C1}. \end{aligned} \tag{3}$$

We tag this interferometry configuration as $\alpha 2$ or Sagnac-$\alpha 2$. With cyclic permutations, we obtain the other two interferometry configurations $\beta 2$ and $\gamma 2$.

1.3 Orbit Configuration for LISA-like Missions

LISA was a mission proposed to ESA and NASA which would use laser links of a nearly equilateral triangle with side 5 Gm for three S/C to observe low-frequency GWs (LISA Study Team 2000). The formation would be inclined by about 60° with respect to the ecliptic trailing the Earth by about 20°, and rotate counterclockwise facing the Sun as shown in Figure 2. This project ended nominally in April, 2011 with NASA's withdrawal.

After the termination of the ESA-NASA collaboration, a scaled-down LISA mission called eLISA/NGO was proposed as a joint effort between seven European countries (France, Germany, Italy, the Netherlands, Spain, Switzerland and the UK) and ESA. The NGO assessment study report received excellent scientific evaluation (`http://eLISA-ngo.org`). The mission configuration consists of a "mother" S/C at one vertex and two "daughter" S/C at two other vertices with the mother S/C optically linked with the two daughter S/C forming an interferometer. The duration of the mission is 2 yr for science orbit and about 4 yr including transferring and commissioning. The mission S/C orbit configuration is similar to LISA, but with a nominal arm length of 1 Gm, inclined by about 60° with respect to the ecliptic and trailing Earth by $10^\circ - 20^\circ$.

Table 1 Comparing the resulting path length differences of the first-generation and $X + Y + Z$ TDI configurations for different arm lengths for various mission proposals: 1 Gm (eLISA), 2.5 Gm (new LISA), 3 Gm (TAIJI) and 5 Gm (classical LISA).

	TDI path length difference ΔL			
First-generation	eLISA [ns]	New LISA [ns]	TAIJI [ns]	Classical LISA [ns]
TDI configuration	[min, max], rms average	[min, max], rms average	[min, max], rms average	[min, max], rms average
X	[−119, 99], 40	[−799, 737], 306	[−1221, 1084], 467	[−3286, 2967], 1417
Y	[−84, 100], 38	[−708, 537], 289	[−1039, 740], 431	[−3543, 3262], 1680
Z	[−90, 106], 37	[−558, 665], 248	[−887, 1030], 380	[−3724, 3096], 1471
$X + Y + Z$	[−0.074, 0.777], 0.243	[−1.754, 4.466], 1.410	[−3.273, 6.243], 1.949	[−15.693, 8.743], 8.757
Sagnac-α	[−1965, −1857], 1906, 20*	[−12309, −11551], 11911, 153*	[−17759, −16623], 17151, 234*	[−49273, −46213], 47644, 715*
Sagnac-β	[−1948, −1855], 1907, 19*	[−12262, −11624], 11915, 144*	[−17666, −16749], 17156, 216*	[−49466, −46101], 47649, 843*
Sagnac-γ	[−1952, −1853], 1906, 18*	[−12199, −11593], 11906, 125*	[−17611, −16661], 17145, 192*	[−49581, −46142], 47610, 746*
Relay-U	[−79, 77], 32	[−502, 467], 222	[−781, 657], 333	[−3479, 2322], 1412
Relay-V	[−102, 80], 34	[−689, 545], 238	[−1069, 776], 367	[−3128, 2507], 1175
Relay-W	[−79, 96], 35	[−666, 596], 271	[−987, 879], 407	[−3167,1933], 1370
Beacon-P	[−60, 49], 20	[−401, 368], 153	[−612, 541], 233	[−1639, 1490], 708
Beacon-Q	[−43, 50], 19	[−356, 267], 145	[−521, 367], 216	[−1770, 1637], 841
Beacon-R	[−46, 53], 19	[−278, 332], 124	[−442, 514], 190	[−1856, 1552], 736
Monitor-E	[−49, 60], 20	[−368, 401], 153	[−541, 612], 233	[−1490, 1639], 708
Monitor-F	[−50, 43], 19	[−267, 356], 145	[−367, 521], 216	[−1637, 1770], 841
Monitor-G	[−53, 46], 19	[−332, 278], 124	[−514, 442], 190	[−1552, 1856], 736
Nominal arm length	1 Gm	2.5 Gm	3 Gm	5 Gm
Mission duration (d)	2200	2200	2200	2200
Requirement on ΔL	10 m (33 ns)	25 m (83 ns)	30 m (100 ns)	50 m (167 ns)

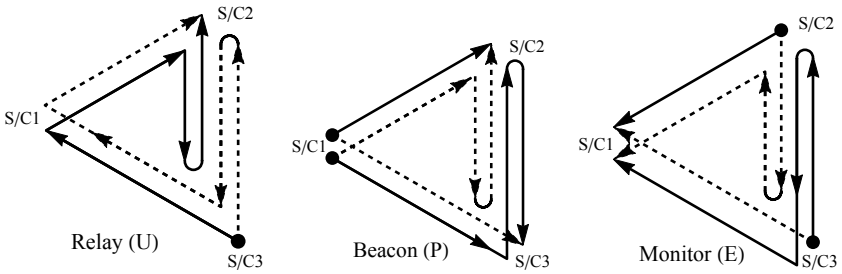

Fig. 1 Interference paths of the 1st-generation TDI for Relay (U), Beacon (P) and Monitor (E) (Vallisneri 2005).

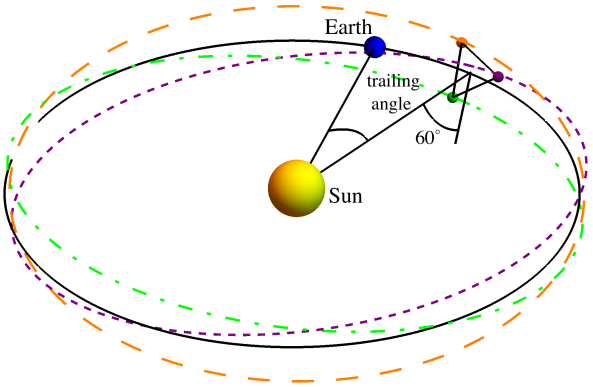

Fig. 2 Schematic of LISA-type orbit configuration in an Earth-like solar orbit.

1.4 TAIJI and New LISA

The Chinese Academy of Sciences initiated the TAIJI program for pre-study of a GW detector in space in 2016 and chose a LISA-like formation with a 3 Gm arm length to study (Hu & Wu 2017, Wu 2018, Guo et al. 2018).

On 2017 January 13, a new LISA proposal was submitted to ESA for the L3 slot of the Cosmic Vision Programme (Amaro-Seoane et al. 2017) and was selected in ESA's Science Programme[1]. The basic concept is like

[1] *http://www.esa.int/Our_Activities/Space_Science/Gravitational_wave_mission_selected_planet-hunting_mission_moves_forward*

that for classical LISA with a down-scaled arm length of 2.5 Gm. Here is a quote from the proposal:

> "...Three independent interferometric combinations of the light travel time between the test masses are possible, allowing, in data processing on the ground, the synthesis of two virtual Michelson interferometers plus a third null-stream, or 'Sagnac' configuration."

The two Michelson interferometers are two TDIs. They could be X, Y or Z if the noise requirement is satisfied. Nevertheless, we will find out that these TDIs do not meet the current noise requirement.

The TDI situation for TAIJI is similar as we will see in the next subsection.

1.5 Comparison of TDIs for Interferometers with Different Arm Lengths

In this paper, we use the CGC 2.7.1 ephemeris (see Wang & Ni 2015) to optimize the orbits and numerically evaluate TDIs. The differences in orbit evolution of Earth calculated using CGC 2.7.1 compared with that using DE430 starting on 2028 March 22 for 2200 d are less than 82 m, 0.32 mas and 0.11 mas for radial distance, longitude and latitude, respectively.

In Table 1, we compile and compare the resulting differences for the first-generation TDIs listed in the Section 1.2.1, i.e. X, Y, Z, $X + Y + Z$ and Sagnac configurations, etc., for TAIJI, new LISA, classical LISA and eLISA. In Table 2, we compile and compare those for the second-generation TDIs listed in Section 1.2.2.

From Table 1, all the first-generation TDIs for LISA-like missions do not satisfy their respective requirements. From Table 2, all the second-generation TDIs for eLISA, new LISA, TAIJI and classical LISA satisfy their respective requirements with good margins. For TAIJI, all the second-generation TDIs satisfy their respective requirements with good margins. To use the first-generation TDIs, requirements must be relaxed with accompanying technology development. To use the second-generation TDIs, the corresponding GW response and sensitivity must be calculated.

In Section 2, we work out a set of 2200-day optimized S/C orbits starting on 2028 March 22 using the CGC 2.7.1 ephemeris framework for TAIJI, new LISA, classical LISA and eLISA. In Section 3, we obtain the numerical results pertaining to the first-generation TDIs for TAIJI and new LISA listed in Table 1. In Section 4, we obtain the numerical results pertaining to the second-generation TDIs for TAIJI and new LISA listed in Table 2. In Section 5, we compare and discuss in detail the resulting differences due to different arm lengths, and conclude this paper with discussion and outlook.

2 TAIJI, NEW LISA, ELISA AND CLASSICAL LISA ORBIT OPTIMIZATIONS

In the LISA-like missions, the distance between any two of the three S/C must be maintained as closely as possible during the geodetic flight to minimize relative Doppler velocities between S/C in order to satisfy respective Doppler frequency requirements. LISA orbit formation has been studied in various previous works (Vincent & Bender 1988; Folkner et al. 1997; Cutler 1998; Hughes 2002; Hechler & Folkner 2003; Dhurandhar et al. 2005; Yi et al. 2008; Li et al. 2008; Dhurandhar et al. 2013). We have used the CGC ephemeris framework together with initial conditions from the DE ephemeris series to optimize the orbits of eLISA/NGO (Wang & Ni 2013a) and a LISA-type mission with 2 Gm nominal arm length (Wang & Ni 2013a) numerically, as well as that of ASTROD-GW (Men et al. 2010b,a; Wang & Ni 2011, 2012, 2013b).

The TAIJI (Hu & Wu 2017) and new LISA (Amaro-Seoane et al. 2017) proposals chose nominal arm lengths of 3 Gm and of 2.5 Gm, respectively. In this section, we describe the procedures for the orbit choice and work out the optimization by taking the examples of the TAIJI proposal. After that, we work out the results for optimized orbits of new LISA, eLISA and classical LISA.

2.1 The Initial Choice of Initial Conditions for TAIJI

There are various ways to choose the orbits of the three S/C so that the orbit configuration satisfies the equal arm length requirement to first order in $\alpha[= l/(2R)]$, the ratio of the planned arm length l of the orbit configuration to twice radius R (1 AU) of the mean Earth orbit. We follow the procedures given in Dhurandhar et al. (2005) and our previous paper Wang & Ni (2013a) to make the initial choice of the initial conditions to start our optimization procedure.

We choose the initial time t_0 for science orbit configuration to be JD2462503.0 (2030-Jan-1st 12:00:00) and work in the heliocentric coordinate system (X, Y, Z) with X-axis in the vernal equinox direction. First, a set of elliptical S/C orbits is defined as in Dhurandhar et al. (2005)

$$\begin{aligned} X_k &= R(\cos\psi_k + e)\cos\epsilon\,, \\ Y_k &= R\sqrt{1-e^2}\sin\psi_k\,, \qquad (k = 1, 2, 3) \\ Z_k &= R(\cos\psi_k + \epsilon)\sin\epsilon\,, \end{aligned} \tag{4}$$

Table 2 Comparison of the resulting path length differences for the second-generation TDIs listed in Section 1.2.2 for 1 Gm (eLISA), 2.5 Gm (new LISA), 3 Gm (TAIJI) and 5 Gm (classical LISA).

	TDI path length difference ΔL			
First-generation	eLISA [ps]	New LISA [ps]	TAIJI [ps]	Classical LISA [ps]
TDI configuration	[min, max], rms average	[min, max], rms average	[min, max], rms average	[min, max], rms average
$[ab, ba]$	[−0.51, 0.45], 0.187	[−8.9, 6.5], 3.2	[−15.8, 11.6], 5.7	[−72, 60], 28
$[cd, dc]$	[−0.44, 0.45], 0.179	[−7.3, 7.4], 3.1	[−12.8, 12.6], 5.4	[−76, 53], 30
$[ef, fe]$	[−0.44, 0.48], 0.182	[−7.1, 7.3], 3.0	[−13.0, 12.6], 5.2	[−73, 62], 28
$[a^2b^2, b^2a^2]$	[−4.1, 3.6], 1.5	[−71, 52], 26	[−126, 93], 45	[−576, 479], 222
$[c^2d^2, d^2c^2]$	[−3.5, 3.5], 1.4	[−58, 59], 24	[−102, 101], 43	[−607, 421], 237
$[e^2f^2, f^2e^2]$	[−3.4, 3.8], 1.5	[−56, 58], 23	[−103, 101], 41	[−578, 494], 221
$[abab, baba]$	[−2.1, 1.8], 0.8	[−36, 26], 13	[−63, 46], 23	[−288, 239], 111
$[cdcd, dcdc]$	[−1.7, 1.8], 0.7	[−29, 30], 12	[−51, 50], 21	[−304, 210], 118
$[efef, fefe]$	[−1.7, 1.9], 0.7	[−28, 29], 12	[−52, 50], 21	[−289, 247], 111
$[ab^2a, ba^2b]$	[−0.01, 0.01], 0.002	[−0.02, 0.01], 0.003	[−0.02, 0.01], 0.003	[−0.02, 0.02], 0.005
$[cd^2c, dc^2d]$	[−0.011, 0.010], 0.002	[−0.012, 0.009], 0.002	[−0.011, 0.010], 0.002	[−0.021, 0.014], 0.004
$[ef^2e, fe^2f]$	[−0.010, 0.013], 0.002	[−0.013, 0.009], 0.002	[−0.017, 0.012], 0.002	[−0.022, 0.014], 0.005
Sagnac-α2	[−0.17, 0.18], 0.07	[−2.7, 3.0], 1.3	[−4.8, 5.2], 2.2	[−23.2, 22.8], 11.2
Sagnac-β2	[−0.17, 0.16], 0.07	[−3.0, 2.6], 1.2	[−5.2, 4.4], 2.1	[−22.7, 24.6], 11.3
Sagnac-γ2	[−0.19, 0.16], 0.07	[−2.9, 2.7], 1.2	[−5.0, 4.9], 2.1	[−26.3, 25.4], 11.1
Nominal arm length	1 Gm	2.5 Gm	3 Gm	5 Gm
Mission duration (d)	2200	2200	2200	2200
Requirement on ΔL	10 m (33 ns)	25 m (83 ns)	30 m (100 ns)	50 m (167 ns)

where for the mission with nominal arm length l equals λ Gm, $e \simeq 0.001925 \times \lambda$; $\epsilon \simeq 0.00333 \times \lambda$; $R = 1$ AU. The eccentric anomaly ψ_k is related to the mean anomaly $\Omega(t - t_0)$, and the Ω is defined as 2π/(one sidereal year). The ψ_k is defined implicitly by

$$\psi_k + e \sin \psi_k = \Omega(t - t_0) - (k-1)\frac{2\pi}{3}, \qquad (5)$$

which is solved by numerical iteration. Define $x_k, y_k, z_k (k = 1, 2, 3)$ to be

$$\begin{aligned} x_k =& X_k \cos\Big[\frac{2\pi}{3}(k-1) + \varphi_0\Big] \\ & - Y_k \sin\Big[\frac{2\pi}{3}(k-1) + \varphi_0\Big], \\ y_k =& X_k \cos\Big[\frac{2\pi}{3}(k-1) + \varphi_0\Big] \\ & + Y_k \sin\Big[\frac{2\pi}{3}(k-1) + \varphi_0\Big], \\ z_k =& Z_k \ , \end{aligned} \qquad (6)$$

where $\varphi_0 = \psi_E - 20^\circ$ and ψ_E is defined to be the position angle of Earth with respect to the X-axis at t_0. The initial conditions in the heliocentric coordinates are

$$\boldsymbol{\mathcal{R}}_{\rm S/Ck} = [x_k, y_k, z_k], \quad (k = 1, 2, 3). \qquad (7)$$

Choosing $t = t_0$, we obtain the initial positions, and calculating the derivatives at $t = t_0$, we obtain the initial velocities. With the choice of t_0 = JD2462503.0 (2030-Jan-1st 12:00:00), the initially chosen orbits have relatively good equal-arm performance until JD2464053.0 (2034-Mar-31st 12:00:00). From the time trend of the performance, we perceived that the orbits would still be rather good when we back evolved the orbit for a period of time; and the result is as expected when the time goes back to JD2461853.0 (2028-Mar-22nd 12:00:00). Thereby, there could be a promising duration of 2200 d for optimization when the mission is set to start from JD2461853.0 (2028-Mar-22nd 12:00:00) with the evolved back initial conditions. For TAIJI, early launch would be desirable and GW observation starting in 2028 could be a possible scenario. For a 2030-start, this 2200 d orbit would also be useful as reference.

Our goal for the orbit optimization is twofold: (i) to equalize the three arm lengths as much as possible for the triangular formation and (ii) to reduce the Doppler velocities between three pairs of S/C. For the TAIJI proposal of 3 Gm arm length, the requirement on the Doppler velocities is below $\pm 6\,\mathrm{m\,s^{-1}}$ between the S/C in order for frequency tracking between S/C to be within ± 6 MHz (for laser light of 1064 nm wavelength) due to Doppler frequency shifts. For TDI, minimizing the Doppler velocities between the S/C also minimizes the path length differences of various TDI configurations. We assume that the requirement on the Doppler velocities is directly proportional to the arm length. For example, for classical LISA with arm length 5 Gm the requirement is $\pm 10\,\mathrm{m\,s^{-1}}$ (LISA Study Team 2000). To accelerate our optimization

program, Runge-Kutta 7th/8th order integration is used to search for the orbit in accordance with the mission requirement. The 4th order Runge-Kutta is used to verify stability after one candidate orbit is achieved.

2.2 The TAIJI Mission Orbit Optimization

The goal of the TAIJI mission orbit optimization is to equalize the three arm lengths of the new LISA formation and to make the relative line-of-sight velocities smaller than $6\,\mathrm{m\,s^{-1}}$ between the three pairs of S/C. Firstly, the initial conditions for the three S/Cs are calculated from the equations in Section 2.1 at JD2462503.0 (2030-Jan-1st 12:00:00) and evolved back to JD2461853.0 (2028-Mar-22nd 12:00:00) using the CGC 2.7.1 ephemeris framework. We list this initial choice of initial states in the third column of Table 3. The TAIJI S/C orbits are then calculated for 2200 d using CGC 2.7.1. The variations of arm lengths and Doppler velocities between the TAIJI S/C are drawn in Figure 3.

As we can see in Figure 3, the Doppler velocity between S/C1 and S/C3 goes slightly beyond $6\,\mathrm{m\,s^{-1}}$. The optimization procedure is to modify the initial heliocentric distances and/or velocities of the S/C. So, we tentatively adjust the initial heliocentric distance of S/C1 to optimize the orbit. The optimized orbit was achieved when the heliocentric distance of S/C1 was decreased by a factor of 2.7×10^{-7}, and the initial conditions are shown in the fifth column of Table 3. Variations of the arm lengths for the final achieved orbit, Doppler velocities, formation angles and the lag angle behind the Earth with the mission time are shown in Figure 4. The variations of arm lengths are within $\pm 1\%$ and velocities in the line-of-sight direction are within the $\pm 6.0\,\mathrm{m\,s^{-1}}$ requirement. The angle between the barycenter of the S/C and Earth in 2200 d starts at 22° behind Earth and varies between 18° and 23° with a quasi-period of variation of about 1 sidereal year due mainly to Earth's elliptic motion.

2.3 The Orbit Optimization for New LISA, eLISA and Classical LISA

For new LISA, classical LISA and eLISA, all with different arm lengths, the goal of the optimization is to make the Doppler velocities under a given prorated requirement as discussed in Section 2.1, that is ± 5, ± 10 and $\pm 2\,\mathrm{m\,s^{-1}}$ respectively. In general, the shorter the arm length for the mission formation is, the easier it is to achieve the optimization (since linear approximation works better). For the 1 Gm arm length mission orbits, the initial conditions specified from the equations in Section 2.1 with back evolution satisfy the requirement that the line-of-sight Doppler velocities be smaller than $\pm 2\,\mathrm{m\,s^{-1}}$ for the period of the mission considered. For new LISA, similar to TAIJI, the orbit configuration meets the mission requirement when the heliocentric distance of S/C1 is decreased by a factor of 3.0×10^{-7}.

With the increase of the arm length to 5 Gm, there are larger nonlinear perturbations on the variation of the arm length. More iterative adjustments are needed to meet the mission requirement. We adjust the heliocentric distances of S/C1 and S/C2 together with the heliocentric velocity of S/C1, before we achieve the final optimized orbit. The scale of the adjustment is on the order of 10^{-6} to 10^{-7} in the ecliptic heliocentric coordinate system. The optimized initial conditions for new LISA, classical LISA and eLISA are shown in Table 4.

The new LISA proposes the configuration lag angle behind the Earth to be around 20° while eLISA/NGO proposed the lag angle to be around 10°. This may make the orbits of the new LISA S/C suffer less gravitational perturbation from the Earth and the orbit configuration can stay stable for more than 6 yr compared to the orbit configuration of eLISA/NGO (Wang & Ni 2013a).

Since the initial condition choices for all missions worked out in this paper share the same epoch and nearly the same barycenter of S/C, there could be some common features when we optimize this family which would be beneficial to our optimization process. We also believe that the optimized orbits we achieved in this paper are definitely not the only choices. These solutions just illustrate the possibilities and what we can achieve and assume. From our previous experiences and present investigation, there should be solutions at any epoch.

3 NUMERICAL SIMULATION OF THE FIRST-GENERATION TDI FOR TAIJI AND NEW LISA

In our early papers (Wang & Ni 2011, 2012), we used the CGC 2.7 ephemeris framework to calculate the difference between the two path lengths for the first-generation TDI configurations of the planar non-precession ASTROD-GW orbit configuration. The results were shown by plotting the difference as a function of the epoch of ASTROD-GW orbit configuration. The method of obtaining these solutions and the TDI configurations was briefly reviewed in Section 1.2.

In the numerical calculation in this section, we calculate the difference between the two path lengths for TDI

Table 3 Initial states (conditions) of three S/C of TAIJI at epoch JD2461853.0 (2028-Mar-22nd 12:00:00) for our initial choice (third column) and after optimizations (fourth column) in the J2000 equatorial (Earth mean equator and equinox) solar-system-barycentric coordinate system.

		Initial choice of S/C initial states		Initial states of S/C after final optimization
S/C1	x	–9.337345684115E–01	adjust to	–9.337343160303E–01
Position	y	3.237549276553E–01	⇒	3.237548395220E–01
(AU)	z	1.426066025785E–01		1.426065637750E–01
S/C1	v_x	–6.034814754038E–03		–6.034814754038E–03
Velocity	v_y	–1.469355864558E–02	=	–1.469355864558E–02
(AU d^{-1})	v_z	–6.554198841518E–03		–6.554198841518E–03
S/C2	x	–9.433977273640E–01		–9.433977273640E–01
Position	y	3.062344469040E–01	=	3.062344469040E–01
(AU)	z	1.411270887844E–01		1.411270887844E–01
S/C2	v_x	–5.861017364349E–03		–5.861017364349E–03
Velocity	v_y	–1.480919323217E–02	=	–1.480919323217E–02
(AU d^{-1})	v_z	–6.298978166673E–03		–6.298978166673E–03
S/C3	x	–9.328957809408E–01		–9.328957809408E–01
Position	y	3.130424089270E–01	=	3.130424089270E–01
(AU)	z	1.255542247698E–01		1.255542247698E–01
S/C3	v_x	–5.949486480991E–03		–5.949486480991E–03
Velocity	v_y	–1.492350292755E–02	=	–1.492350292755E–02
(AU d^{-1})	v_z	–6.408454202380E–03		–6.408454202380E–03

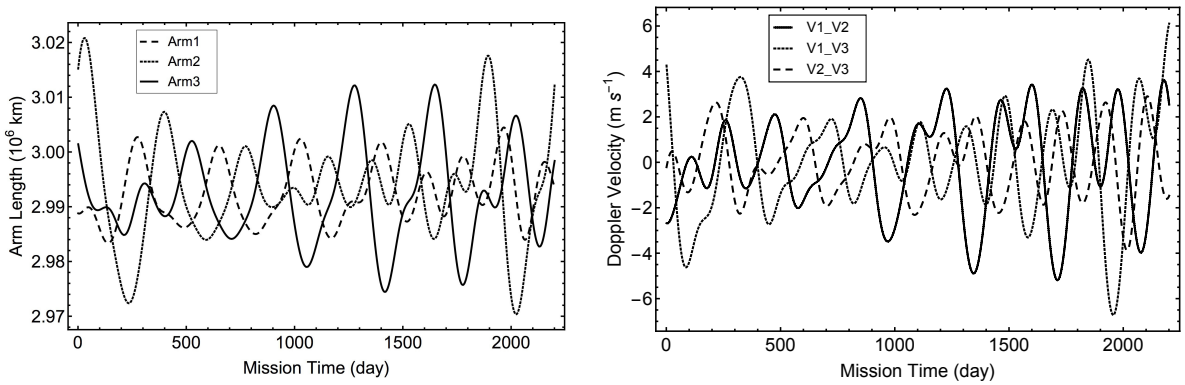

Fig. 3 Variations of the arm lengths and the velocities in the line-of-sight direction in 2200 d for the TAIJI S/C configuration with initial conditions given in column 3 (initial choice) of Table 3.

configurations and plot the difference as a function of the signal arriving epoch of TDI in the first-generation TDI configurations – Michelson (X, Y, Z); Sagnac (α, β, γ); Relay (U, V, W); Beacon (P, Q, R); Monitor (E, F, G) for TAIJI and new LISA. We use the iteration and interpolation methods (Chiou & Ni 2000, 2004; Newhall 1989; Li & Tian 2004) to calculate the time in the barycentric coordinate system as in our early papers. We do this for TAIJI in Section 3.1 and for the new LISA mission in Section 3.2.

3.1 Numerical Results of the First-Generation TDI for TAIJI

In this subsection, we draw the optical path length differences versus time epoch for the Unequal arm Michelson (X, Y, Z) TDIs and their sum $X + Y + Z$ in Figure 5 and other first-generation TDI configurations in Figure 6 for TAIJI with arm length 3 Gm.

3.2 Numerical Results of the First-Generation TDI for New LISA

For new LISA, the optical path length differences versus time epoch for the Unequal arm Michelson (X, Y, Z) TDIs and their sum $X+Y+Z$ have been shown in Figure 7, and other first-generation TDI configurations have been shown in Figure 8.

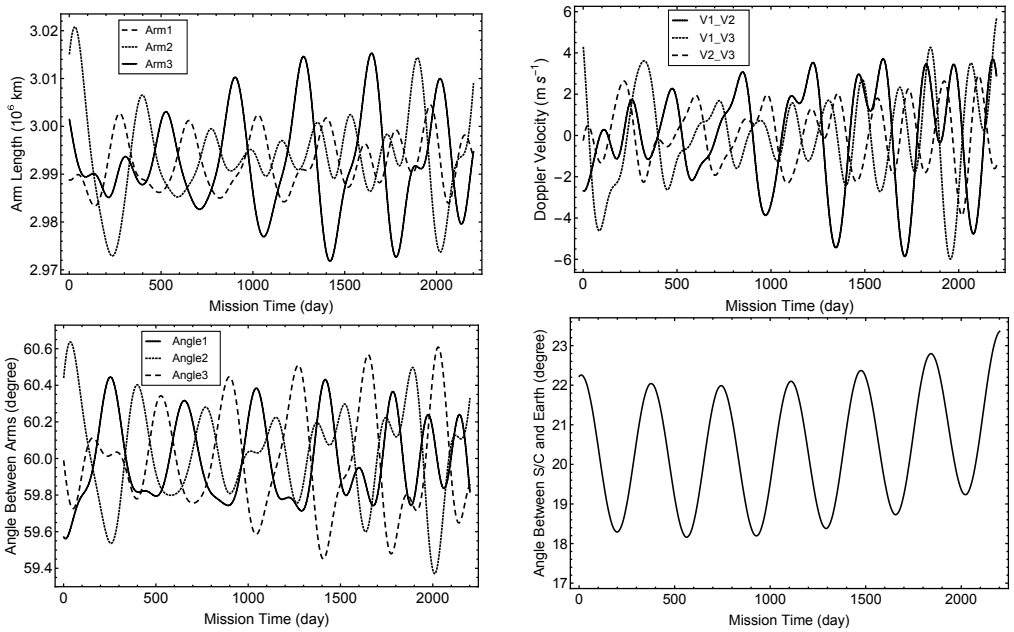

Fig. 4 Variations of the arm lengths, velocities in the line-of-sight direction, formation angles and angle between barycenter of the S/Cs and Earth in 2200 d for the TAIJI S/C configuration with initial conditions given in column 5 (after optimization) of Table 3.

Table 4 Initial conditions of three S/C for optimized eLISA with arm length 1 Gm, for optimized new LISA with arm length 2.5 Gm and optimized classical LISA with arm length 5 Gm at epoch JD2461853.0 (2028-Mar-22nd 12:00:00) in J2000 equatorial (Earth mean equator and equinox) solar-system-barycentric coordinate system.

Arm Length		x (AU)	y (AU)	z (AU)
		v_x (AU d^{-1})	v_y (AU d^{-1})	v_z (AU d^{-1})
1 Gm	S/C1	–9.357297393390E–01	3.175249022108E–01	1.384166686585E–01
		–5.977487755471E–03	–1.477105821259E–02	–6.465498086333E–03
	S/C2	–9.389558953532E–01	3.116740035186E–01	1.379265627712E–01
		–5.919394364688E–03	–1.480954135324E–02	–6.380065664383E–03
	S/C3	–9.354523832766E–01	3.139517985143E–01	1.327436476580E–01
		–5.948925229945E–03	–1.484735001743E–02	–6.416821125538E–03
2.5 Gm	S/C1	–9.337343160303E–01	3.237548395220E–01	1.426065637750E–01
		–6.034814754038E–03	–1.469355864558E–02	–6.554198841518E–03
	S/C2	–9.433977273640E–01	3.062344469040E–01	1.411270887844E–01
		–5.861017364349E–03	–1.480919323217E–02	-6.298978166673E–03
	S/C3	–9.328957809408E–01	3.130424089270E–01	1.255542247698E–01
		–5.949486480991E–03	–1.492350292755E–02	–6.408454202380E–03
5 Gm	S/C1	–9.317122569544E–01	3.299269994748E-01	1.468818648738E–01
		–6.091593636329E–03	–1.461494061048E–02	–6.642025921601E–03
	S/C2	–9.477904576171E–01	3.007808152754E–01	1.444007020429E–01
		–5.802751784201E–03	–1.480798178629E–02	–6.218468839601E–03
	S/C3	–9.303038243396E–01	3.120850334818E–01	1.184065522341E–01
		–5.949986166082E–03	–1.499996136965E–02	–6.399606859148E–03

4 NUMERICAL SIMULATION OF THE SECOND-GENERATION TDI FOR TAIJI AND NEW LISA

In this section, we do the numerical simulation for the second-generation TDIs listed in Section 1.2.2. We plot the optical path length differences versus time epoch of these second-generation TDIs for TAIJI in Section 4.1 and for new LISA in Section 4.2.

From the last diagram in Figure 9 and 11, we notice that the accuracy of the TDI calculation for the path difference should be better than 3 μm (10 fs).

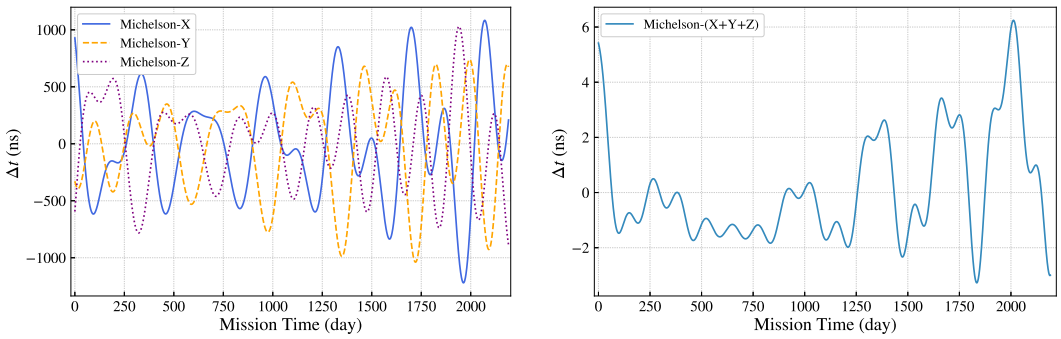

Fig. 5 The optical path length differences for Unequal arm Michelson (X, Y, Z) TDIs (*left*) and their sum $X+Y+Z$ (*right*) for TAIJI. There is a clear cancelation of optical path length differences by 2 orders of magnitude in the sum.

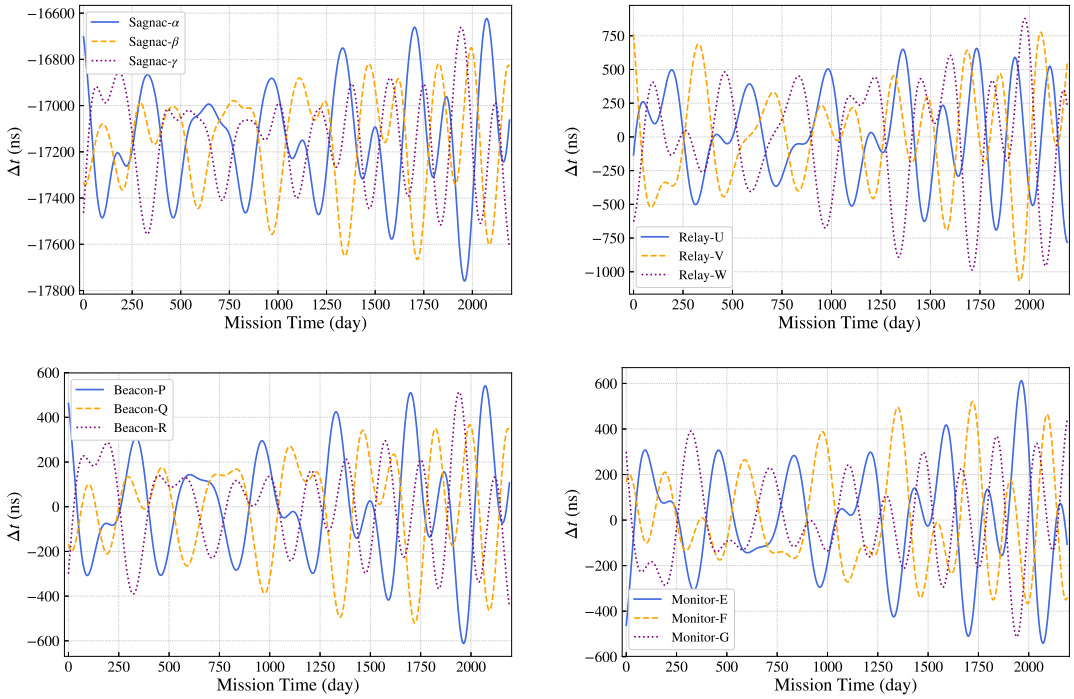

Fig. 6 The optical path length differences for Sagnac (α, β, γ); Relay (U, V, W); Beacon (P, Q, R); Monitor (E, F, G) TDIs for TAIJI.

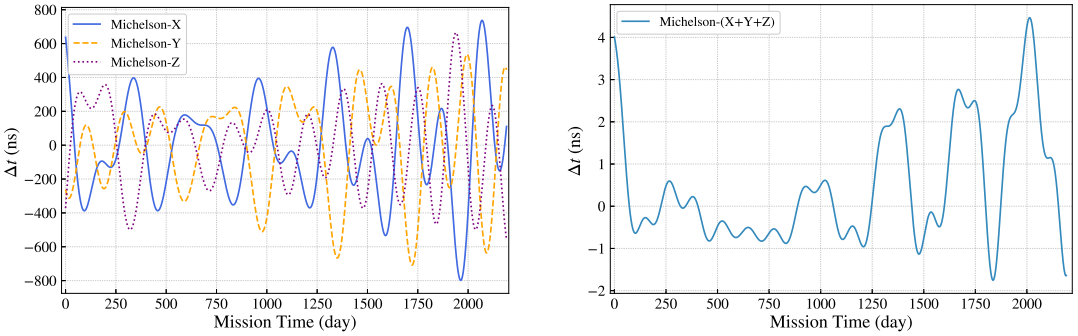

Fig. 7 The optical path length differences for Unequal arm Michelson (X, Y, Z) TDIs (*left panel*) and their sum $X+Y+Z$ (*right panel*) for new LISA. There is a clear cancelation of optical path length differences by 2 orders of magnitude in the sum.

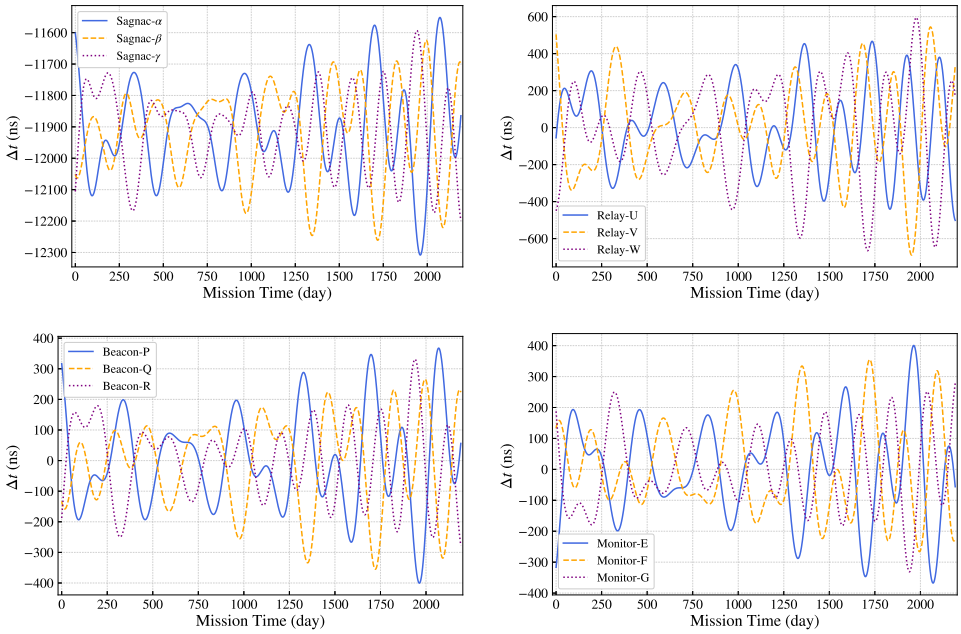

Fig. 8 The optical path length differences for Sagnac (α, β, γ); Relay (U, V, W); Beacon (P, Q, R); Monitor (E, F, G) TDIs for new LISA.

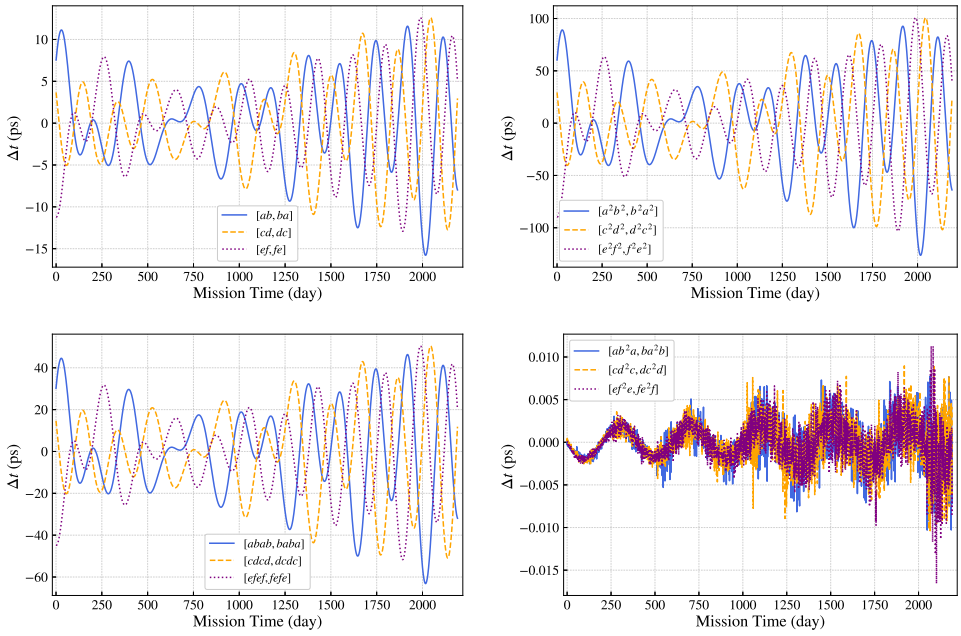

Fig. 9 The difference of two optical path lengths vs. time epoch for $[ab, ba]$, $[cd, dc]$ and $[ef, fe]$ TDI configurations ($n = 1$), and for all $n = 2$ TDI configurations for TAIJI.

4.1 Numerical Results of the Second-Generation TDIs Listed in Section 1.2.2 for TAIJI

For TAIJI having 3 Gm arm length, we show the optical path length differences versus time epoch for $n = 1$ and $n = 2$ configuration TDIs in Figure 9, and the Sagnac $\alpha 2$, $\beta 2$ and $\gamma 2$ TDI configurations in Figure 10.

4.2 Numerical Results of the Second-Generation TDIs Listed in Section 1.2.2 for New LISA

For new LISA with 2.5 Gm arm length, we show the optical path length differences versus time epoch for $n = 1$ and $n = 2$ configuration TDIs in Figure 11, and the Sagnac $\alpha 2$, $\beta 2$ and $\gamma 2$ TDI configurations in Figure 12.

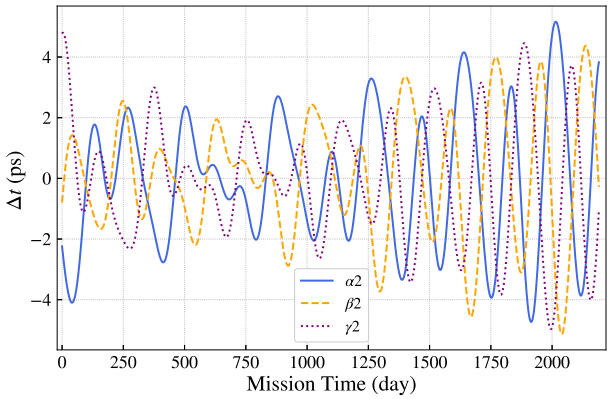

Fig. 10 The difference of two optical path lengths vs. time epoch for Sagnac-type $\alpha 2$, $\beta 2$ and $\gamma 2$ TDIs for TAIJI.

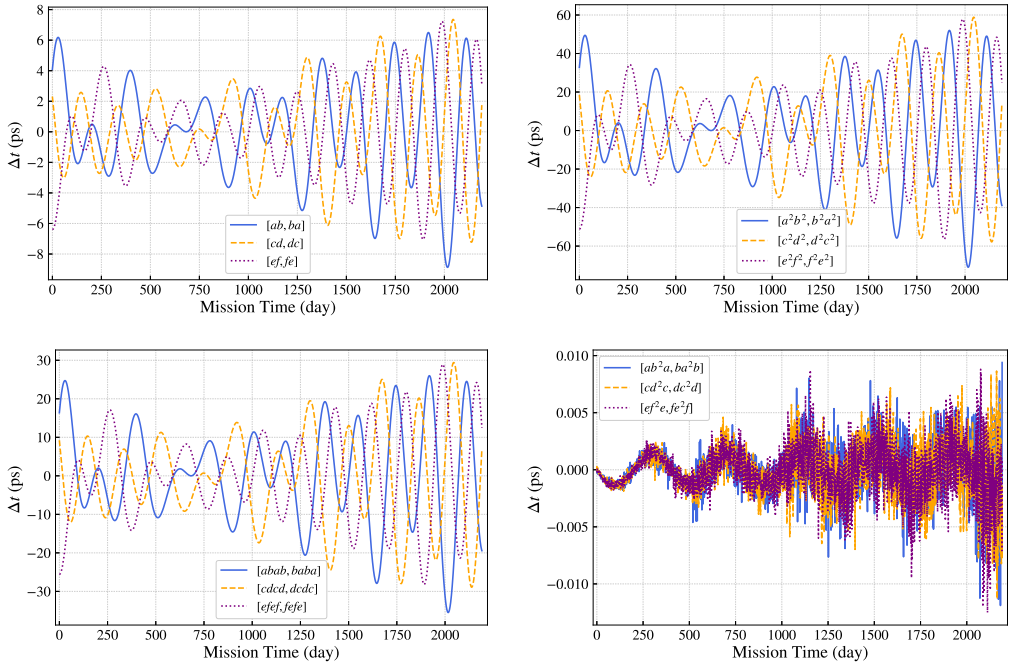

Fig. 11 The difference of two optical path lengths vs. time epoch for $[ab, ba]$, $[cd, dc]$ and $[ef, fe]$ TDI configurations ($n = 1$), and for all $n = 2$ TDI configurations for new LISA.

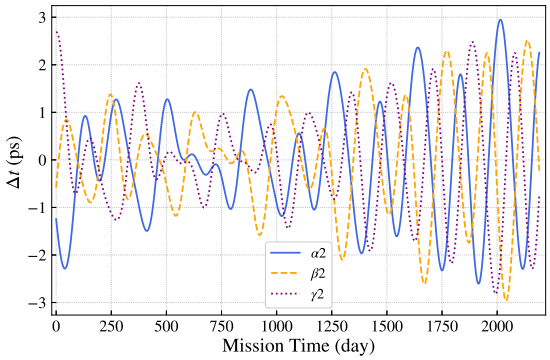

Fig. 12 The difference of two optical path lengths vs. time epoch for Sagnac-type $\alpha 2$, $\beta 2$ and $\gamma 2$ TDIs for new LISA.

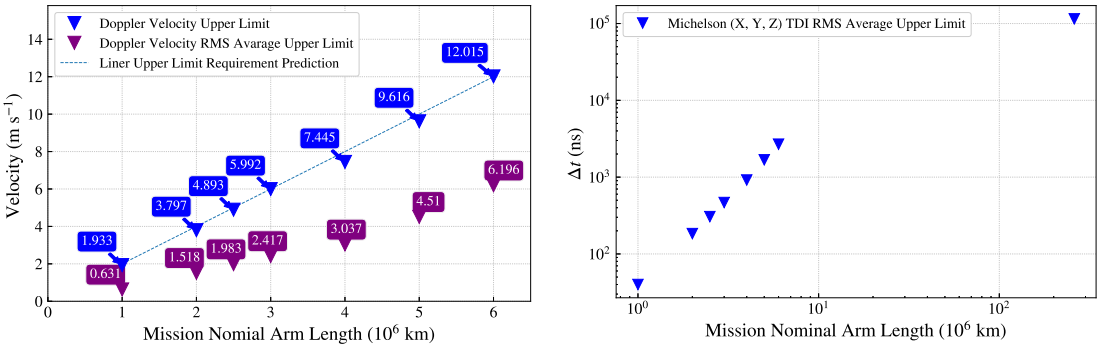

Fig. 13 *Left panel*: Line-of-sight Doppler velocities (maximum and rms average in 2200 d) vs. arm length. *Right panel*: The largest of the rms averages of X, Y and Z TDIs vs. arm length.

5 DISCUSSION AND OUTLOOK

We have optimized a set of 6-year (2200-day) TAIJI and new LISA mission orbits numerically using an ephemeris framework starting on 2028 March 22. The line-of-sight Doppler velocities satisfy the respective requirements. The maximum magnitude and rms magnitude together with the upper-limit requirement versus arm length are plotted in the left panel of Figure 13. In Figure 13, we also plot those of LISA-like interferometers of arm lengths 1 Gm (eLISA), 2 Gm, 4 Gm, 5 Gm (classical LISA) and 6 Gm from Wang & Ni (2017). The upper-limit follows a linear trend. We calculate optical path length differences of various first-generation and second-generation TDIs for these mission orbits and compile them in Table 1 and Table 2 for easy comparison. We list the presently recommended requirement in the last row of the tables. From the tables and the figures in Sections 3 and 4, we can draw the following conclusions:

(1) All the first-generation TDIs violate their respective requirements. For eLISA with arm length 1 Gm, the deviation for X, Y and Z TDIs could be up to a factor of 3.6; for the new LISA case with 2.5 Gm arm length, a factor of 9.6; for TAIJI case with 3 Gm arm length, a factor of 12.5; for classical LISA with 5 Gm arm length, a factor of 22.3. If X, Y and Z TDIs are used for the GW analysis, either the TDI requirement needs to be relaxed by the same factor or the laser frequency stability requirement needs to be strengthened by this factor. In the right panel of Figure 13, we plot the largest value of the rms averages of X, Y and Z TDIs versus arm length. It looks like a power law dependence with power index of about 2.3 on the arm length.

(2) From Table 1, all the first-generation TDIs do not satisfy their respective requirements. From Table 2, all the second-generation TDIs for eLISA, new LISA, TAIJI and classical LISA satisfy their respective requirements with good margins. Hence, to use the first-generation TDIs, the requirement must be relaxed with accompanying technology development. To use the second-generation TDIs, the corresponding GW response and sensitivity must be calculated and applied for the GW data analysis.

(3) Experimental demonstration of TDI in the laboratory for LISA was implemented in 2010–2012 (de Vine et al. 2010; Mitryk et al. 2012). Therefore, the requirement of TDI for TAIJI, eLISA and ASTROD-GW which is based on the LISA requirement is essentially demonstrated. Considering the current development progress of laser technology, the laser frequency noise requirement may be achieved to compensate for 1–2 order TDI relaxation in 10 yr. For TAIJI and new LISA, the X, Y and Z TDIs could still be considered if this development were realized and could be used for one-order more stringent mission requirement.

(4) An optimistic observation start date for TAIJI and new LISA could be in 2028. For other starting dates, similar orbits could be worked out.

Acknowledgements GW receives funding in support of his work leading to these results from the People Programme (Marie Curie Actions) of the European Union's Seventh Framework Programme FP7/2007-2013/ (PEOPLE-2013-ITN) under REA grant agreement n [606176]. It reflects only the authors' view and the Union is not liable for any use that may be made of the information contained therein. WTN would like to thank Rong-Gen Cai for his hospitality at KITPC while writing up part of this work.

References

Abbott, B. P., Abbott, R., Abbott, T. D., et al. 2016a, Physical Review Letters, 116, 241103

Abbott, B. P., Abbott, R., Abbott, T. D., et al. 2016b, Physical Review Letters, 116, 061102

Abbott, B. P., Abbott, R., Abbott, T. D., et al. 2017a, Physical Review Letters, 118, 221101

Abbott, B. P., Abbott, R., Abbott, T. D., et al. 2017b, ApJ, 851, L35

Abbott, B. P., Abbott, R., Abbott, T. D., et al. 2017c, Physical Review Letters, 119, 141101

Abbott, B. P., Abbott, R., Abbott, T. D., et al. 2017d, Physical Review Letters, 119, 161101

Amaro-Seoane, P., Audley, H., Babak, S., et al. 2017, arXiv:1702.00786

Armano, M., Audley, H., Auger, G., et al. 2016, Physical Review Letters, 116, 231101

Armstrong, J. W., Estabrook, F. B., & Tinto, M. 1999, ApJ, 527, 814

Chiou, D.-W., & Ni, W.-T. 2000, Advances in Space Research, 25, 1259

Chiou, D.-W., & Ni, W.-T. 2004, astro-ph/0407570

Cutler, C. 1998, Phys. Rev. D, 57, 7089

de Vine, G., Ware, B., McKenzie, K., et al. 2010, Physical Review Letters, 104, 211103

Dhurandhar, S. V., Nayak, K. R., Koshti, S., & Vinet, J.-Y. 2005, Classical and Quantum Gravity, 22, 481

Dhurandhar, S. V., Nayak, K. R., & Vinet, J.-Y. 2010, Classical and Quantum Gravity, 27, 135013

Dhurandhar, S. V., Ni, W.-T., & Wang, G. 2013, Advances in Space Research, 51, 198

Dick, G. J., Tu, M., Strekalov, D., Birnbaum, K., & Yu, N. 2008, Interplanetary Network Progress Report, 175, 1

Folkner, W. M., Hechler, F., Sweetser, T. H., Vincent, M. A., & Bender, P. L. 1997, Classical and Quantum Gravity, 14, 1405

Francis, S. P., Lam, T. T.-Y., McKenzie, K., et al. 2014, Optics Letters, 39, 5251

Gerberding, O., Sheard, B., Bykov, I., et al. 2013, Classical and Quantum Gravity, 30, 235029

Guo, Z.-K., Cai, R.-G., & Zhang, Y.-Z. 2018, arXiv:1807.09495

Hechler, F., & Folkner, W. M. 2003, Advances in Space Research, 32, 1277

Hu, W.-R., & Wu, Y.-L. 2017, Natl. Sci. Rev., 4, 685

Hughes, S. P. 2002, Preliminary Optimal Orbit Design for the Laser Interferometer Space Antenna (LISA), Tech. rep., NASA Goddard Space Flight Center, Breckenridge, CO; United States

Kawamura, S., Nakamura, T., Ando, M., et al. 2006, Classical Quantum Gravity, 23, S125

Kawamura, S., Ando, M., Seto, N., et al. 2011, Classical and Quantum Gravity, 28, 094011

Kuroda, K., Ni, W.-T., & Pan, W.-P. 2015, International Journal of Modern Physics D, 24, 1530031

Li, G., & Tian, L. 2004, Publications of Purple Mountain Observatory, 23, 160

Li, G., Yi, Z., Heinzel, G., et al. 2008, International Journal of Modern Physics D, 17, 1021

Liao, A.-C., Ni, W.-T., & Shy, J.-T. 2002a, Publications of the Yunnan Observatory, 91, 88

Liao, A.-C., Ni, W.-T., & Shy, J.-T. 2002b, International Journal of Modern Physics D, 11, 1075

LISA Study Team. 2000, LISA (Laser Interferometer Space Antenna): A Cornerstone Mission for the Observation of Gravitational Waves, Tech. Rep. 11, ESA-SCI

Men, J.-R., Ni, W.-T., & Wang, G. 2010a, Chinese Astronomy and Astrophysics, 34, 434

Men, J. R., Ni, W. T., & Wang, G. 2010b, Acta Astronomica Sinica, 51, 198

Mitryk, S. J., Mueller, G., & Sanjuan, J. 2012, Phys. Rev. D, 86, 122006

Newhall, X. X. 1989, Celestial Mechanics, 45, 305

Ni, W.-T. 1997, in Gravitational Wave Detection, ed. K. Tsubono, M.-K. Fujimoto, & K. Kuroda, 20, 117

Ni, W.-T., Shy, J.-T., Tseng, S.-M., et al. 1997, in Proc. SPIE, 3116, Small Spacecraft, Space Environments, and Instrumentation Technologies, eds. F. A. Allahdadi, E. K. Casani, & T. D. Maclay, 105

Tinto, M., & Dhurandhar, S. V. 2014, Living Reviews in Relativity, 17, 6

Vallisneri, M. 2005, Phys. Rev. D, 72, 042003

Vincent, M. A., & Bender, P. L. 1988, in Astrodynamics 1987, ed. P. F. Wercinski, 1346

Wang, G., & Ni, W. T. 2011, Acta Astronomica Sinica, 52, 427

Wang, G., & Ni, W.-T. 2012, Chinese Astronomy and Astrophysics, 36, 211

Wang, G., & Ni, W.-T. 2013a, Classical and Quantum Gravity, 30, 065011

Wang, G., & Ni, W.-T. 2013b, Chinese Physics B, 22, 049501

Wang, G., & Ni, W.-T. 2015, Chinese Physics B, 24, 059501

Wang, G., & Ni, W.-T. 2017, arXiv:1707.09127

Wu, Y.-L. 2018, arXiv:1805.10119

Yi, Z., Li, G., Heinzel, G., et al. 2008, International Journal of Modern Physics D, 17, 1005